Applied Surface Science 405 (2017) 412–419

Contents lists available at ScienceDirect

Applied Surface Science

journal homepage: www.elsevier.com/locate/apsusc

Full Length Article

Low-temperature (75 °C) solid-state reaction enhanced by less-crystallized nanoporous PbI_2 films for efficient $CH_3NH_3PbI_3$ perovskite solar cells

Huifeng Zheng[a,b], Yangqiao Liu[a,c,*], Jing Sun[a,**]

[a] State Key Laboratory of High Performance Ceramics and Superfine Microstructure, Shanghai Institute of Ceramics, Chinese Academy of Sciences, 1295 Dingxi Road, Shanghai 200050, PR China
[b] University of Chinese Academy of Sciences, 19 Yuquan Road, Beijing 100049, PR China
[c] Suzhou Institute of SICCAS (Shanghai Institute of Ceramics, Chinese Academy of Sciences), 238 North Changchun Road, Taicang 215499, Jiangsu Province, PR China

ARTICLE INFO

Article history:
Received 6 December 2016
Received in revised form 7 February 2017
Accepted 8 February 2017
Available online 12 February 2017

Keywords:
Perovskite solar cells
Low-temperature annealing
Solid-state reaction
Nanoporous PbI_2
Non-radiative defects

ABSTRACT

Organohalide perovskite films are usually prepared with the solid-state reaction at a high temperature ≥100 °C, which causes the increase of non-radiative defects and decomposition of perovskite films. Here, we demonstrate it's feasible to prepare high-quality perovskite films with the solid-state reaction method even at a temperature of 75 °C, when enhanced by less-crystallized nanoporous PbI_2 (ln-PbI_2) films. The replacement of compact PbI_2 (c-PbI_2) by ln-PbI_2, results in a significant improvement of crystallinity of perovskite films, besides the elimination of remnant PbI_2. As a result, ln-PbI_2 based perovskite solar cells display much higher power conversion efficiency (PCE) and better stability. Moreover, annealing duration was found to be critical for high PCE and was optimized as 60 min. Finally, with the optimal process, the champion device displayed a PCE of 13.8% and the average PCE reached 10.1% with a satisfactory deviation. Furthermore, we found annealing at high temperature (140 °C) led to a lower PCE compared with that annealed at 75 °C, because non-radiative defects increased significantly during high-temperature annealing. This work may open up a promising avenue for preparing high-quality perovskite films with the low-temperature solid-state reaction method, which is desirable for real application.

1. Introduction

Organometal halide perovskite solar cells (PSCs) have been a hot topic in the field of photovoltaic research since 2012. During the past five years, its power conversion efficiency (PCE) has improved sharply from 9.7% to over 20% [1–5]. The dramatic improvement of PCE mainly comes from the great strides made in the preparation methods of fabricating high quality perovskite films, namely compact, pinhole-free and PbI_2-free perovskite films [3,6–8]. Among them, the two-step solution deposition method is widely used, because it offers more controllable morphology than the one-step method [3,9,10]. Whereas, the conventional two-step dipping method, in which PbI_2 films are dipped into CH_3NH_3I (MAI) solution to react, is notorious for failing in complete conversion of PbI_2 into perovskite, especially in planar PSCs [3,11–13]; on the other hand, dipping too long will result in abnormally large grains on the surface [14–16]. That leads to a dilemma between the conversion completeness and controlled morphology.

To solve the problem, with some modifications to the two-step dipping method, a class of methods based on solid-state reaction have been proposed, in which PbI_2 films react with MAI solid rather than MAI solution [17–20]. However, for all those methods, a high temperature ≥100 °C is often needed to drive the reaction to happen, which is not desirable for energy-saving. More importantly, Peng et al. demonstrated that non-radiative defects of perovskite film increased significantly at higher growth temperature, deteriorating the photovoltaic performance [21]. In addition, some reports have shown that high-temperature annealing will lead to the decomposition of perovskite and presence of remnant PbI_2, which deteriorates the photovoltaic performance, stability and reproducibility [11,22,23]. In a word, it's meaningful to prepare perovskite films with the solid-state reaction method at a much

* Corresponding author at: State Key Laboratory of High Performance Ceramics and Superfine Microstructure, Shanghai Institute of Ceramics, Chinese Academy of Sciences, 1295 Dingxi Road, Shanghai 200050, PR China.
** Corresponding author.
E-mail addresses: yqliu@mail.sic.ac.cn (Y. Liu), jingsun@mail.sic.ac.cn (J. Sun).

http://dx.doi.org/10.1016/j.apsusc.2017.02.057
0169-4332/

lower temperature; however, to our best knowledge, no concerning study has been reported thus far.

Taken into account the reaction mechanism of those solid-state reaction methods, a layer of MAI is usually stacked on a compact PbI_2 (c-PbI_2) layer, in which the reaction is realized through a long-range interdiffusion between PbI_2 and MAI [17,19,20]. However, the diffusion is ineffective due to the lack of kinetically favorable van der Waals gap in the formed $CH_3NH_3PbI_3$ interlayer between MAI and PbI_2 [24,25]. As a result, to enhance the diffusion, high temperature annealing is always applied in solid-state reaction for preparing perovskite films [25,26]. In short, the necessity of high-temperature annealing in the conventional solid-state reaction, lies in the long distance for diffusion. Therefore, instead of elevating the reaction temperature to accelerate the diffusion, shortening the distance for diffusion is another choice, while avoiding the negative effects of high-temperature annealing. That can be realized by the application of nanoporous PbI_2 (n-PbI_2) films in the solid-state reaction: the diffusion distance in the case of n-PbI_2 film will be reduced to the size of PbI_2 particles rather than the thickness of entire PbI_2 layer. Moreover, many reports have shown that the n-PbI_2 will facilitate the reaction between PbI_2 and MAI, as much larger reaction interface is present in a n-PbI_2 film than the conventional compact one [11,12,15,23,27].

In our previous work, we developed a facile way to prepare n-PbI_2 films with the antisolvent-solvent extraction method [15]. In this work, however, we managed to fabricate a new type of n-PbI_2 with much worse crystallinity by omitting the post-annealing process of PbI_2 films after preparation, which is desirable for energy-saving. Moreover, we found that the less-crystallized nanoporous PbI_2 (ln-PbI_2) film was able to convert into perovskite film more rapidly, compared with the well-crystallized nanoporous PbI_2 (wn-PbI_2, with post-annealing). It can be ascribed to the fact that good crystallinity of PbI_2 will retard the conversion of PbI_2 into perovskite [22,28,29].

Here, we apply ln-PbI_2 films to realize effective low-temperature solid-state reaction (LT-SSR). The replacement of c-PbI_2 by ln-PbI_2, leads to better crystallized and PbI_2-free perovskite films, compared with the PbI_2-remained films based on c-PbI_2. Resultantly, those ln-PbI_2 based PSCs deliver both of much higher PCE and better stability in ambient air, as the remnant PbI_2 plays an important role in the deterioration of c-PbI_2 based samples. Furthermore, the annealing duration was optimized, which was found to be a critical factor to obtain efficient PSCs. With the optimal process, a champion PCE of 13.8% was obtained and the average PCE of 70 samples reached 10.1% with a satisfactory deviation. Additionally, compared with the sample prepared at 75 °C, non-radiative defects increased significantly when the sample was prepared at 140 °C. As a result, the champion PCE of 140 °C decreased to 11.8% from 13.8% (75 °C).

2. Experimental section

2.1. Materials and reagents

MAI was prepared in-house according to the procedure reported in literature [25]. PbI_2, anhydrous chlorobenzene, Li-bis(trifluoromethanesulfonyl)imide (Li-TFSI) and 4-*tert*-butylpridine (t-BP) were obtained from Sigma-Aldrich. 2,2′,7,7′-Tetrakis[N,N−di(4-methoxyphenyl)amino]-9, 9′,-spirobifluorene (Sipro-MeOTAD) and Tris(2-(1H−pyrazol-1-yl) -4-*tert*-butylpyridine)-cobalt(III)Tris(bis(trifluoromethylsulfonyl) imide)) (FK209 Co(III) TFSI salt) were purchased from Luminescence Technology Corp., Taiwan. Both of dimethylformamide (DMF) and 2-propanol (IPA) were dehydrated by molecular sieves (4A) before use.

2.2. Device fabrication

Fluorine-doped tin oxide (FTO; 15 Ω sq^{-1}, Nippon Sheet Glass) glass substrates were patterned by etching with Zn powder and diluted HCl solution. The patterned FTO substrates were cleaned with ultrasonication sequentially in detergent (Hellmanex II, 2%), water, ethanol, acetone and ethanol, respectively. Then those cleaned FTO substrates were treated with ultraviolet (UV) for 15 min before being coated with a compact TiO_2 layer by spin-coating a yellowish solution of tetrabutyl titanate [30]. After drying at 70 °C, they were annealed at 500 °C for 30 min. Then, the films were treated with $TiCl_4$ solution (40 mM, 70 °C) for 30 min, and rinsed with deionized water and ethanol before being annealed at 500 °C for another 30 min.

When cooled down, the substrates were treated with UV for 15 min again, before the deposition of perovskite layer. Specifically, a layer of PbI_2 was prepared by spin-coating 1 M PbI_2 solution (in DMF kept at 70 °C) at 3000 r.p.m, from which the c-PbI_2 films were obtained by drying at 70 °C; while wn-PbI_2 and ln-PbI_2 films were fabricated with additional antisolvent-solvent extraction process developed by our group, and post-annealing was conducted on wn-PbI_2 but not on ln-PbI_2 [15]. Finally, perovskite films were obtained by sequentially spin-coating of 8 mg/ml and 30 mg/ml MAI solution (in IPA) onto those PbI_2 films and annealing at 75 °C or 140 °C for varied duration. For annealing at 140 °C, the duration was shortened to 20 min to avoid the decomposition of perovskite films. For the two-step dipping method, perovskite films were fabricated by dipping ln-PbI_2 films into MAI solution (10 mg/ml in IPA) for several minutes. Then, those perovskite films were washed by IPA and annealed at 75 °C, unless stated otherwise.

The hole-transporting layer (HTL) was fabricated by spin-coating of a solution of Spiro-MeOTAD (72.3 mg/ml) at 4000 r.p.m for 30 s with a recipe as reported [3], and was oxidized in a desiccator overnight. At last, a layer of Ag (~100 nm) was evaporated onto the top of HTL, with an effective area of 0.15 cm^2 for device. For preparing perovskite layer and HTL, all the procedures were conducted inside an Ar-filled glovebox.

2.3. Measurement and characterization

X-ray diffraction (XRD) spectra were obtained from Rigaku D/max 2550 V (using Cu Kα radiation, with a step size of 0.02°). A field emission scanning electron microscopy (FESEM; SU8220, Hitachi) was used to characterize the morphology of perovskite films and conduct Energy Dispersive X-Ray Spectroscopy (EDS) test. A UV/Vis/NIR spectrophotometer (Lambda 950, Perkin Elmer) was used to measure the absorption spectra of $CH_3NH_3PbI_3$ films. Photoluminescence (PL) measurement was conducted on a spectrometer (FLS 980, Edinburg Instruments). The topography of perovskite films was measured in the tapping mode with an atomic force microscope (AFM; ScanAsyst, Veeco Dimension Icon). Under the simulated AM 1.5G illumination (100 mW/cm^2; Oriel Sol3A Class AAA Solar Simulator, Newport), the *J-V* curves of PSCs were recorded by a Keithley 2400 source meter through reverse scan (1 V to −0.1 V) with a step size of 11 mV and delay time of 20 ms. And the simulated illumination had been calibrated by an optical power meter (Newport, 1918-R) before each test. An incident photon-to-electron conversion efficiency (IPCE) test system (Zahner, CIMPS-pcS3/IPCE) was used to measure IPCE spectra. Electrochemical Impedance spectroscopy (EIS) were recorded by an electrochemical workstation (CHI660D, CH Instruments) under simulated AM 1.5G illumination, in the frequency range from 1 MHz to 1 HZ. The measurement of photovoltaic performance (*J-V* curves and EIS) was conducted at room temperature with a controlled relative humidity (RH) of 20%.

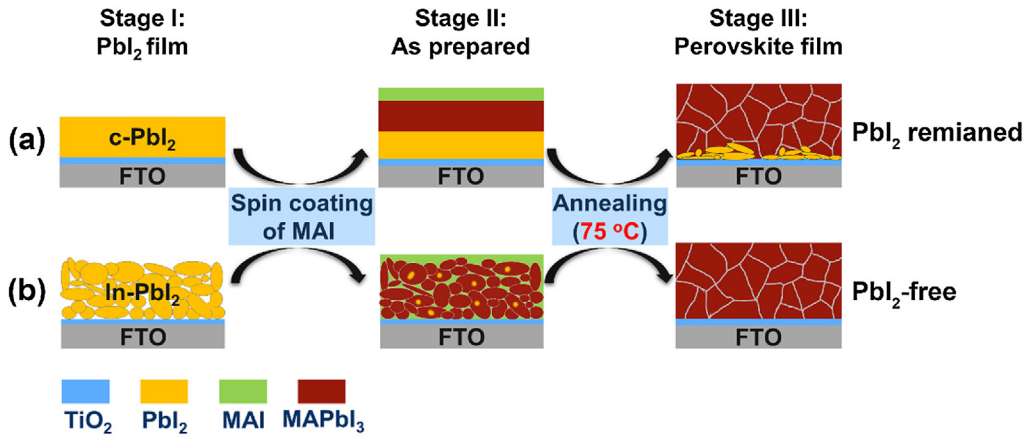

Fig. 1. Schematic illustration of preparing perovskite films by the LT-SSR method based on different types of PbI_2: (a) c-PbI_2, (b) ln-PbI_2.

3. Results and discussion

3.1. Advantages of ln-PbI_2 over c-PbI_2

Fig. 1 schematically shows the process of preparing perovskite films by the LT-SSR method. The c-PbI_2 film was prepared in the conventional way, in which the film was annealed directly after the spin-coating of PbI_2 solution; while the ln-PbI_2 film was fabricated using the antisolvent-solvent extraction method reported by our previous work, except that the post-annealing of nanoporous PbI_2 was eliminated in this work [15]. The elimination of annealing resulted in a much worse crystallinity which was reported to be beneficial for conversion of PbI_2 into perovskite, though the morphology was similar to the annealed one (Fig. S1a–c) [22,28,29]. Consequently, as depicted in Fig. S1d, ln-PbI_2 is able to convert into $CH_3NH_3PbI_3$ faster compared with wn-PbI_2. When those PbI_2 films were sequentially spin coated with a combination of low and high concentration of MAI solution, $CH_3NH_3PbI_3$ films were obtained after being annealed at 75 °C for varied duration.

Fig. 2 compares the differences between ln-PbI_2 and c-PbI_2 films and their distinct behavior during the conversion into $CH_3NH_3PbI_3$ films. The ln-PbI_2 film is nanoporous, while the c-PbI_2 film is really compact, as shown in Fig. 2a and d. Additionally, both types of PbI_2 films display a strong (001) peak of PbI_2 (near 12.66°); how-

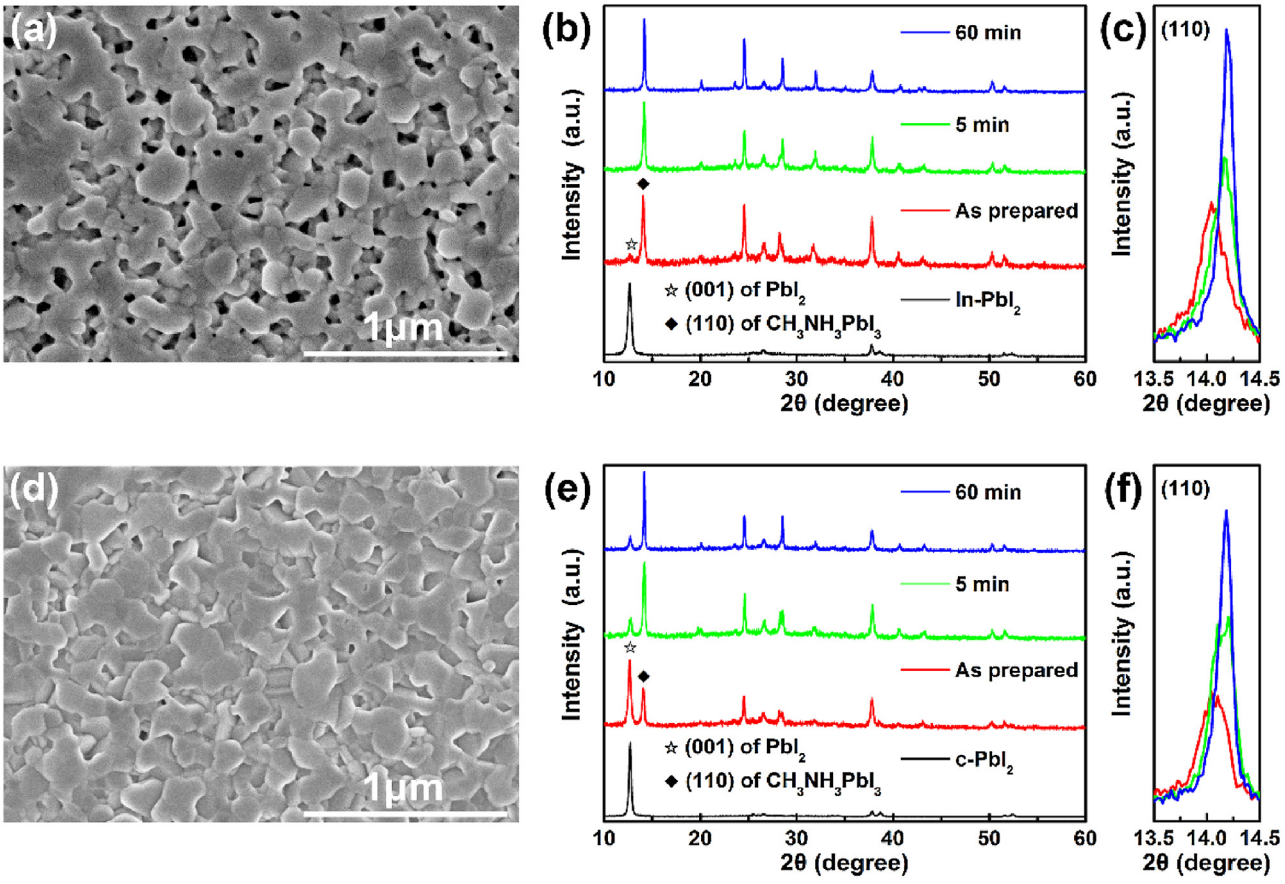

Fig. 2. SEM images of (a) ln-PbI_2 and (d) c-PbI_2. XRD spectra of films at different preparation stages based on (b)(c) ln-PbI_2, (e)(f) c-PbI_2.

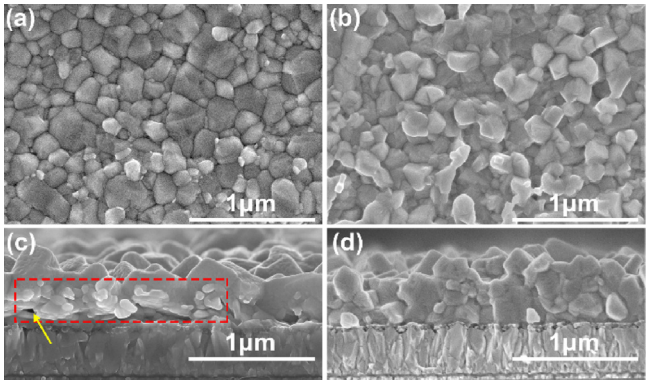

Fig. 3. SEM images of perovskite films based on (a)(c) c-PbI_2, (b)(d) ln-PbI_2, which were annealed for 60 min at 75 °C.

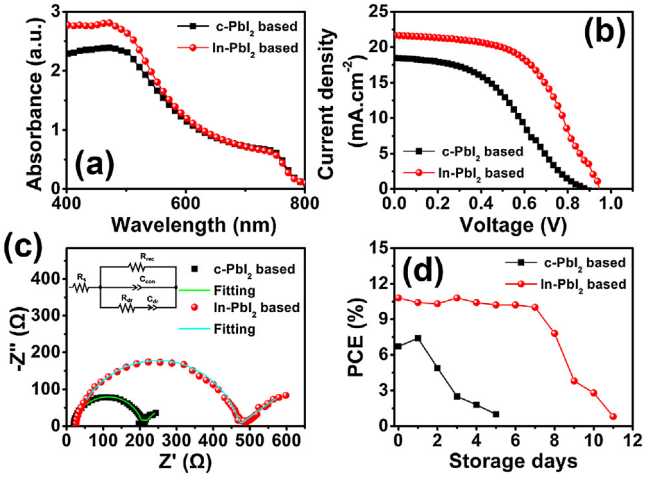

Fig. 4. (a) UV–vis spectra of perovskite films based on different types of PbI_2. (b) *J-V* curves, corresponding (c) Nyquist plots (the best samples in the same batch) and (d) device stability of PSCs based on different types of PbI_2.

ever, the ln-PbI_2 film (0.386°) delivers a smaller full width at half maximum (FWHM) than that of the c-PbI_2 one (0.268°), indicating a worse crystallinity of ln-PbI_2. Consequently, as depicted in Fig. 2b and e, ln-PbI_2 is able to convert into $CH_3NH_3PbI_3$ much faster compared with c-PbI_2, due to its synergetic effect of nanoporous morphology and worse crystallinity [12,15,28,29]. Fig. 2b shows the evolution of phase composition with the reaction going on, based on ln-PbI_2 films. Surprisingly, the as prepared film based on ln-PbI_2 only shows a weak (001) peak of PbI_2 even without any annealing (Fig. 2b), indicating the fast conversion of PbI_2 into $CH_3NH_3PbI_3$. When annealed at 75 °C for only 5 min, the characteristic peak of PbI_2 disappears completely, implying a PbI_2-free $CH_3NH_3PbI_3$ film is obtained. When extending the duration to 60 min, the crystallinity of perovskite film gets better, as indicated by the sharper (110) peak (Fig. 2c). Contrastively, the conversion of PbI_2 into $CH_3NH_3PbI_3$ based on the c-PbI_2 film is less complete, as shown in Fig. 2e. The (001) peak of remnant PbI_2 is more significant in the as prepared film based on c-PbI_2, compared with that of the ln-PbI_2 based one. Though the crystallinity of $CH_3NH_3PbI_3$ film improves apparently by extending the annealing duration, significant PbI_2 still remains when annealed for 60 min (Fig. 2e and f). Additionally, the crystallinity of perovskite film based on ln-PbI_2 is better than that of the c-PbI_2 based one, as indicated by a smaller FWHM for the ln-PbI_2 based sample (0.139°) than that of the one based on c-PbI_2 (0.154°). The purer phase and better crystallinity of perovskite film in the case of ln-PbI_2 compared with that based on c-PbI_2, mainly comes from the nanoporous morphology of PbI_2 which facilitates the homogenization process.

The morphology of perovskite films based on c-PbI_2 and ln-PbI_2 were compared as well, displayed in Fig. 3. Both kinds of perovskite film consist of polycrystals, whose average sizes are similar, as shown in the top-view SEM images (Fig. 3a and b); in addition, both films deliver similar RMS roughness as well (Fig. S2). However, the perovskite film based on ln-PbI_2 seems more compact than that of the c-PbI_2 based one, indicated by its more ambiguous grain boundaries (Fig. 3b). On the other hand, those perovskite films differ much in the morphology of cross-section, as displayed in Fig. 3c and d. For the c-PbI_2 based one, the top layer is a compact perovskite layer; however, an additional layer of remnant PbI_2 is present between the perovskite and compact TiO_2 layer, as indicated by those relatively brighter nanoplates in Fig. 3c (marked by the red dashed box) [31,32]. That was confirmed by EDS test, as depicted in Fig. S3. The remnant PbI_2 was reported to hinder the transfer of electron from perovskite into TiO_2 layer [11,33,34]. Additionally, the perovskite film based on c-PbI_2 is not totally compact due to the incomplete conversion of PbI_2, as labelled by the yellow arrow (Fig. 3c). Contrastively, the ln-PbI_2 based perovskite film mainly consists of several stacking layers of small grains; and no remnant PbI_2 is observed, agreeing with the XRD result (Fig. 2b). Moreover, the cross-section of ln-PbI_2 based perovskite film is very compact, without the presence of any pinholes, as shown in Fig. 3d.

It is worth noting that, with the two-step dipping method [3], it's facile to fabricate perovskite films at low-temperature (75 °C) as well; however, the quality of those films is much worse than those prepared by the LT-SSR method, as indicated by Fig. S4. Specifically, when dipped too short, PbI_2 doesn't convert into $CH_3NH_3PbI_3$ completely and the resultant perovskite film is far from compact (Fig. S4a and c); while dipped too long, many micron-sized grains are present on the surface (Fig. S4b). It demonstrates the advantages of LT-SSR method over the two-step dipping method in controlling perovskite film's morphology and the conversion completeness.

Furthermore, we compared the absorption spectra of those perovskite films based on different types of PbI_2, as shown in Fig. 4a. Specifically, ln-PbI_2 based perovskite film delivers higher absorbance than that of the c-PbI_2 based one in the range from 400 nm to 600 nm, while their absorbances are similar above 600 nm. However, it will not affect the J_{sc} apparently because their light-harvesting efficiencies are almost identical, as depicted in Fig. S5. The lower absorbance of the c-PbI_2 based one mainly results from the incomplete conversion of PbI_2 into $CH_3NH_3PbI_3$, as shown in Figs. 2e and 3c. Then, both types of perovskite films were fabricated into PSCs with a setup of FTO/compact TiO_2/$CH_3NH_3PbI_3$/Spiro-MeOTAD/Ag. For the c-PbI_2 based ones, most samples deliver considerably low efficiency (below 5%); while the ln-PbI_2 based ones show much better performance. Here, the champion samples of each group are displayed in Fig. 4b. The c-PbI_2 based sample show a V_{oc} of 0.888 V, little lower than that of the ln-PbI_2 based one (0.939 V). Meanwhile, the differences of J_{sc} and *FF* between these two samples are more significant. The J_{sc} of the ln-PbI_2 based sample (21.6 mA cm^{-2}) is over 3 mA cm^{-2} higher than that of the c-PbI_2 based one (18.5 mA cm^{-2}); while the *FF* of the c-PbI_2 based one only reaches 40.8%, 25% relatively lower than its counterpart based on ln-PbI_2 (54.2%). Therefore, the ln-PbI_2 based champion device delivers a PCE of 11.0%, 64% relatively higher than that of the c-PbI_2 based one (6.7%). The lower performance of the c-PbI_2 based samples can be ascribed to two factors: Firstly, the crystallinity of c-PbI_2 based perovskite films are worse than that of ln-PbI_2 based ones, as indicated in the XRD test mentioned previously, which will deteriorate the photovoltaic performance [35]. Secondly, the remnant PbI_2 interlayer between $CH_3NH_3PbI_3$ and TiO_2 will inhibit the injection of electron from $CH_3NH_3PbI_3$ into TiO_2 layer [11,33,34], which was confirmed by the EIS test as well

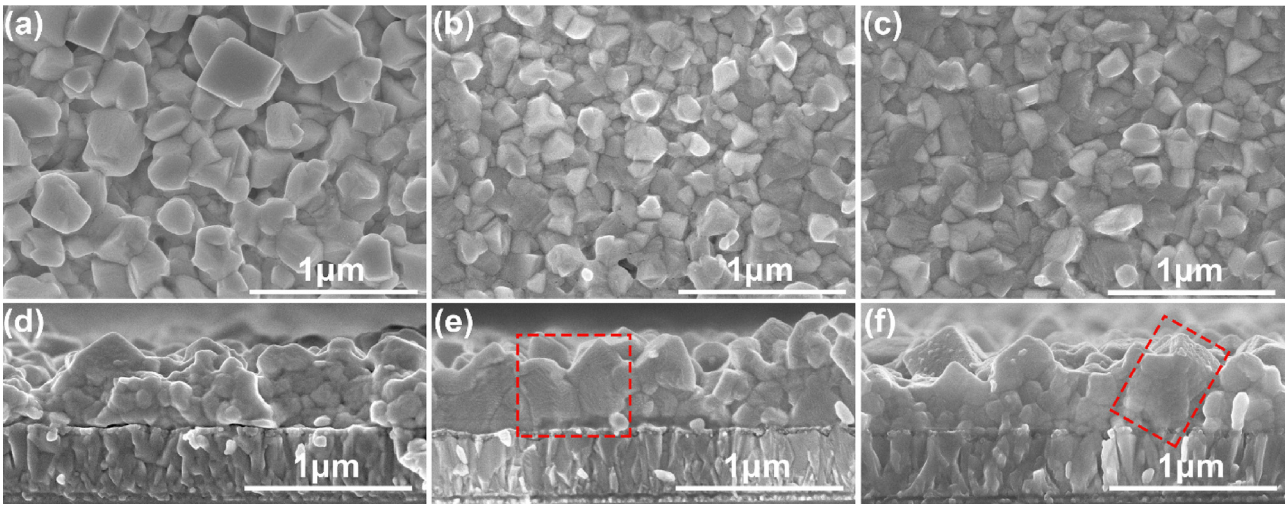

Fig. 5. SEM images of perovskite films with varied annealing duration: (a)(d) 30 min, (b)(e) 60 min, (c)(f) 120 min.

(Fig. 4c). According to Cheng's theory, the high-frequency features of Nyquist plots should be attributed to the charge recombination across the perovskite/contact interfaces in planar PSCs [36]. As displayed in Fig. 4c, the Nyquist plots can be fitted well by Cheng's model. Based on it, we can infer that the charge recombination resistance (high-frequency semicircle) of the c-PbI_2 based one (0.40 kΩ) is much lower than that of the one based on ln-PbI_2 (1.58 kΩ), indicating an easier recombination across the interface of $CH_3NH_3PbI_3$ (PbI_2)/TiO_2 for the c-PbI_2 based one. It mainly comes from the inhibited injection of electron by the remnant PbI_2 interlayer, intensifying the recombination near the interface [11].

Moreover, we compared the stability of the samples from those two groups. All the samples were tested without encapsulation in ambient air (~30% RH, 27 °C). As shown in Fig. 4d, the PCE of the c-PbI_2 based sample drops sharply in the first three days, while the ln-PbI_2 based one can stabilize for one week. The worse stability of the c-PbI_2 based sample should be attributed to the remnant PbI_2 as well, as demonstrated by others [23,37]. On the other hand, even the ln-PbI_2 based sample delivers a worse stability compared with other reports [11,23]. That may come from the application of a more reactive electrode of Ag rather than Au [11,23,38], which will accelerate the degradation process by consuming HI (the byproduct of the decomposition of $CH_3NH_3PbI_3$) and shifting the equilibrium of the decomposition reaction to the side of products [38].

3.2. Optimization of annealing duration

In order to increase PCE further, the annealing duration was optimized. Firstly, we observed the evolution of perovskite film's morphology with the annealing duration (from 30 min to 120 min), as displayed in Fig. 5. As the top-view images show, all the perovskite films are compact, pinhole-free, consisting of polycrystals whose sizes are around 200 nm. Due to annealing at a low temperature (75 °C), no significant grain growth was observed during the extension of annealing duration from 30 min to 120 min; on the contrary, some grains of the perovskite film annealed for 30 min are surprisingly little larger than those with longer annealing duration (60 min and 120 min), as depicted in Fig. 5a–c. That may result from the grain growth during the stage of IPA washing, as more MAI tends to remain on the surface when annealed for shorter duration, with which more additional MAI solution will form on the surface (during this stage) to facilitate the grain growth of $CH_3NH_3PbI_3$. Furthermore, as the AFM test shows, the perovskite film of 60 min delivers the lowest RMS (Fig. S2b and S6), indicating the smoothest surface which is desirable for efficient PSCs [39]. On the other hand, the cross-sections of those films are similar as well, mainly consisting of several stacking layers of small grains (Fig. 5d–f). However, some grains reach a size as large as film's thickness in both films annealed for 60 min and 120 min (labelled by the red dashed boxes), which are absent in the case of 30 min. It indicates that grain growth of $CH_3NH_3PbI_3$ in the thickness direction is possible even when annealed at a temperature as low as 75 °C, which can be ascribed to the facilitation of grain growth by the setup of MAI evenly distributed inside an ln-PbI_2 film.

Meanwhile, XRD characterization was conducted to monitor the changes of phase composition and crystallinity when extending the annealing duration. Fig. 6a shows that all those perovskite films are PbI_2-free and display the same characteristic peaks, with 14.20°, 20.13°, 23.62° and 24.61° assigned to (110), (200), (211) and (202) crystal planes of $CH_3NH_3PbI_3$ (tetragonal phase), respectively [40]. That demonstrates the advantage of LT-SSR method applied here, as several reports have proved $CH_3NH_3PbI_3$ film is facile to decompose into PbI_2 even annealed for short duration at high temperature [31,41]. On the other hand, the FWHM of (110) peak varies much with the duration, as shown in Fig. 6b. Specifically, the FWHM is 0.162°, 0.139° and 0.180° for 30 min, 60 min and 120 min, respectively. That means the perovskite film annealed for 60 min delivers the best crystallinity, which is desirable for efficient PSCs [35].

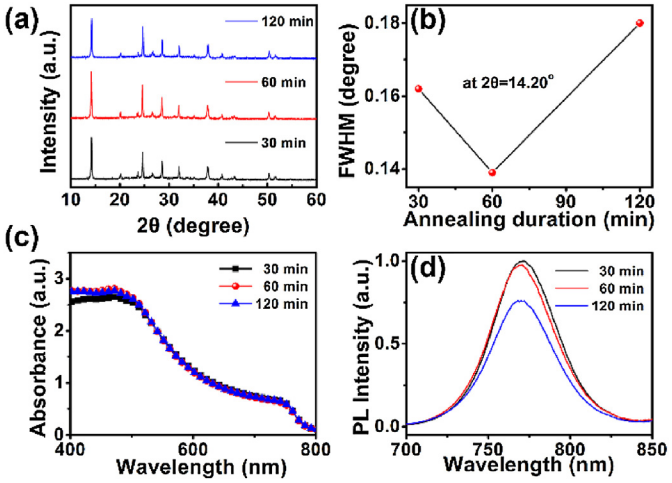

Fig. 6. Effects of annealing duration on (a) XRD spectra, (b) FWHM, (c) UV–vis spectra and (d) PL spectra.

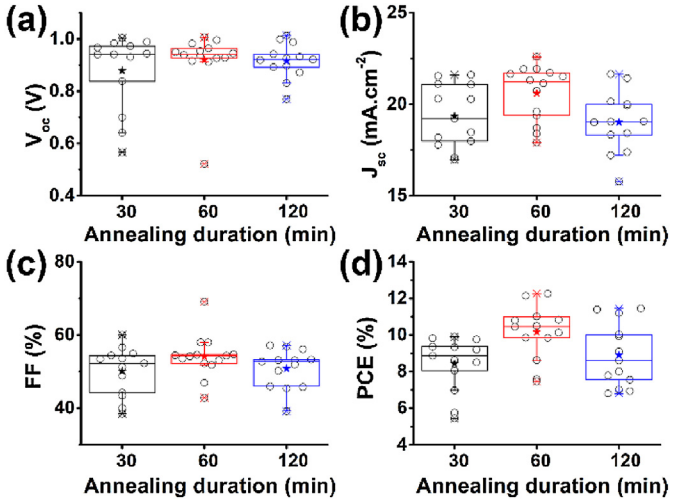

Fig. 7. Effects of annealing duration on the photovoltaic performance: (a) V_{oc}, (b) J_{sc}, (c) *FF*, (d) *PCE*. Solid stars are mean values, while hollow circles represent raw data.

The deterioration of crystallinity, during the extension of annealing duration from 60 min to 120 min, may indicate some kinds of defects generate when annealed too long.

As the morphology (Fig. 5) and XRD spectra (Fig. 6a) do not vary much for those samples with different annealing duration, the UV–vis spectra do not change apparently (Fig. 6c), either. Furthermore, PL spectra were characterized in order to study the effect of annealing duration on the density of non-radiative defects. As depicted in Fig. 6d, all the samples show a strong PL peak around 770 nm, in accordance with other reports [21,42]. For the samples annealed for 30 min and 60 min, the PL intensities are comparative; however, when further extending the annealing duration to 120 min, the PL intensity drops to only 75% of that of the sample annealed for 30 min. That suggests long-time annealing, even at a temperature as low as 75 °C, will lead to a significant increase of non-radiative defects, which will deteriorate the photovoltaic performance [21]. Those defects probably contribute to the decrease of crystallinity for the sample of 120 min as well, as indicated in Fig. 6b.

Then, we compared the photovoltaic performance of those three groups based on varied annealing duration, as displayed in Fig. 7. When the annealing duration extends from 30 min to 60 min, the average V_{oc}, J_{sc} and *FF* improve a bit, from 0.878 V, 19.4 mA cm^{-2} and 50.1% to 0.920 V, 20.6 mA cm^{-2} and 54.1% (Table S1), respectively. As a result, the average PCE rises from 8.4% to 10.2%. The improvement of photovoltaic performance can be ascribed to two aspects: enhanced crystallinity [35] and smoother surface [15,43] of $CH_3NH_3PbI_3$ film annealed for 60 min. When further prolonging the duration to 120 min, a slight drop is observed in all average parameters, as shown in Fig. 7 and Table S1. Therefore, the average PCE decreases to only 8.9% (120 min) from 10.2% (60 min). The sharp fall of photovoltaic performance mainly comes from the increase of non-radiative defects during the extension of duration to 120 min, which cause sever recombination (as indicated by the PL spectra in Fig. 6d). Hence, annealing for 60 min is the optimal preparation process.

Fig. 8a displays the typical setup of planar PSC fabricated with the optimal process, in which the perovskite layer is about 320 nm with a slight variation in thickness. The uniformity in thickness is critical to high photovoltaic performance and reproducibility [6]. In order to display the merits of the low-temperature solid-state reaction, we compared the champion devices of low-temperature (75 °C for 60 min) and high-temperature (140 °C for 20 min) annealing. As shown in Fig. 8b, the device prepared at 75 °C delivers a PCE of 13.8%, with a J_{sc} of 22.5 mA cm^{-2}, V_{oc} of 0.956 V and *FF* of 64.2%; while its counterpart prepared at 140 °C only shows a champion PCE of 11.8%, with a J_{sc} of 22.4 mA cm^{-2}, V_{oc} of 0.866 V and *FF* of 60.6%. The significant lower PCE of 140 °C based sample mainly results from the loss in V_{oc} and *FF*, which indicates a severer recombination in the case of high-temperature annealing compared with the low-temperature one. That was confirmed by the PL spectra test, as displayed in Fig. 8c. The PL intensity of the sample prepared at 140 °C, is only 23% as high as that of the sample annealed at 75 °C, demonstrating more non-radiative recombination defects generate during the high-temperature annealing which will deteriorate the photovoltaic performance [21]. To exclude the effect of crystallinity and phase purity, XRD spectrum of the sample annealed at

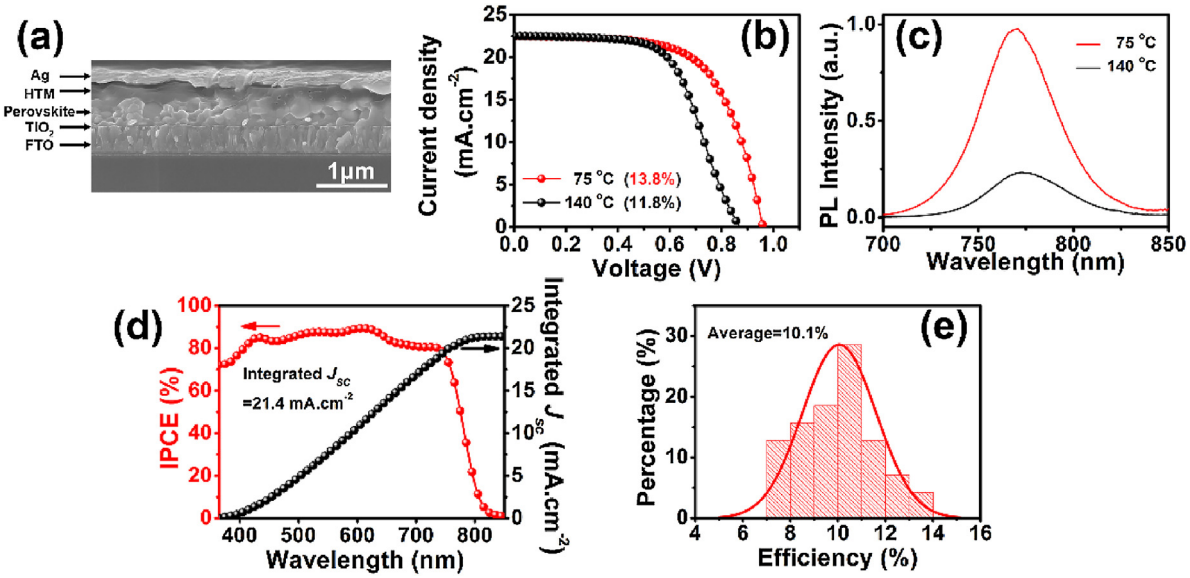

Fig. 8. (a) Setup of planar PSCs in which the perovskite layer was annealed for 60 min at 75 °C. (b) *J-V* curves (champion devices in each group) and (c) PL spectra of samples prepared at 75 °C (60 min) and 140 °C (20 min), respectively. (d) IPCE and the corresponding integrated J_{sc} of the champion device prepared at 75 °C (60 min). (e) Statistics on power conversion efficiency based on the optimal process (75 °C × 60 min, 70 devices).

140 °C is provided in Fig. S7a. The spectrum suggests that the sample prepared at 140 °C seems to be pure-phase perovskite, without any visible PbI_2; moreover, the crystallinity of the perovskite film annealed at 140 °C is better than that annealed at 75 °C, indicated by a smaller FWHM (0.111°) than that of the low-temperature one (0.139°). The non-radiative defects probably originate from the slight decomposition of perovskite layer on the surface during high-temperature annealing, as indicated by those tiny bright particles present at grain boundaries, as displayed in Fig. S7b [32].

Additionally, the *J-V* curves of the champion device (75 °C × 60 min) are displayed in Fig. S8, with varied scanning directions and scanning rates. The reverse scan delivers a PCE of 13.8%, higher than that under forward scan (10.5%), displaying scan-direction-dependent hysteresis (Fig. S8a). On the other hand, the PCE is independent of scan-rate when changing the dwell time from 10 ms to 100 ms, as shown in Fig. S8b. This phenomenon of scanning-parameters-dependent *J-V* curves is frequently reported in PSCs, whose origin is still not clear [44,45]. Moreover, the IPCE spectrum of the best sample (75 °C × 60 min) is presented in Fig. 8d, which shows a strong response (with efficiency over 80%) in the range from 408 nm to 737 nm and peaks at 89.4% (610 nm). Resultantly, the integrated J_{sc} reaches as high as 21.4 mA cm^{-2}, in good accordance with that measured from the *J-V* curve (22.5 mA cm^{-2}). Furthermore, the PCE distribution of 70 samples prepared with the optimal process is shown in Fig. 8e, whose average efficiency reaches 10.1% with a deviation of 1.6%. It demonstrates the desirable reproducibility of this method, namely, the low-temperature solid-state reaction enhanced by ln-PbI_2 films.

4. Conclusion

In summary, low-temperature (75 °C) solid-state reaction has been demonstrated to be able to prepare high quality perovskite films, when enhanced by ln-PbI_2 films. The results indicate ln-PbI_2 films are superior to c-PbI_2 films when applied in the LT-SSR method, resulting in more complete conversion into better crystallized $CH_3NH_3PbI_3$ films. As a result, the champion PCE of the ln-PbI_2 based PSC (11%) is 64% relatively higher than its counterpart based on c-PbI_2 (6.7%). In addition, the c-PbI_2 based PSC displays a much worse stability in ambient air, compared with that of the one based on ln-PbI_2, due to the negative effect of remnant PbI_2. Moreover, we thoroughly investigated the effects of annealing duration on the properties and photovoltaic performance of $CH_3NH_3PbI_3$ films. Surprisingly, we found that annealing for 60 min was the best: too short duration would lead to a rough surface and worse crystallinity, while annealing too long would result in the increase of non-radiative defects. With the optimal process, the champion device delivered a PCE of 13.8% and the average PCE reached 10.1%. Additionally, the device prepared with this low-temperature method delivers a much better photovoltaic performance, compared with those annealed at high-temperature (140 °C), because the non-radiative defects are effectively inhibited by avoiding annealing at a high-temperature. This work proves the feasibility of preparing high quality $CH_3NH_3PbI_3$ films at low temperature (75 °C) with the solid-state reaction method when enhanced by ln-PbI_2 films. Moreover, it demonstrates the merits of this low-temperate method, compared with the conventional high-temperature one, which is able to inhibit the generation of non-radiative defects and is more energy-saving. Due to the difficulty of effective grain growth at low-temperature in solid-state reaction, the performance based on this method is still behind some high-temperature ones [17,19]. However, with some modification to accelerate the grain growth, this low-temperature method will fabricate PSCs as efficient as those prepared at high temperature.

Acknowledgement

This work was supported by the National Basic Research Program of China (2012CB932303), the National Natural Science Foundation of China (Grant No. 61574148, 51272265), Taicang Key R&D Projects (TC2016SF09) and the State Key Laboratory for Modification of Chemical Fibers and Polymer Materials, Donghua University (No. LK1517).

Appendix A. Supplementary data

Supplementary data associated with this article can be found, in the online version, at http://dx.doi.org/10.1016/j.apsusc.2017.02.057.

References

[1] H. Kim, C. Lee, J. Im, K. Lee, T. Moehl, A. Marchioro, S. Moon, R. Humphry-Baker, J. Yum, J.E. Moser, M. Graetzel, N. Park, Lead iodide perovskite sensitized all-solid-state submicron thin film mesoscopic solar cell with efficiency exceeding 9%, Sci. Rep. 2 (2012) 591.
[2] M.M. Lee, J. Teuscher, T. Miyasaka, T.N. Murakami, H.J. Snaith, Efficient hybrid solar cells based on meso-superstructured organometal halide perovskites, Science 338 (2012) 643–647.
[3] J. Burschka, N. Pellet, S. Moon, R. Humphry-Baker, P. Gao, M.K. Nazeeruddin, M. Gratzel, Sequential deposition as a route to high-performance perovskite-sensitized solar cells, Nature 499 (2013) 316–319.
[4] W.S. Yang, J.H. Noh, N.J. Jeon, Y.C. Kim, S. Ryu, J. Seo, S.I. Seok, High-performance photovoltaic perovskite layers fabricated through intramolecular exchange, Science 348 (2015) 1234–1237.
[5] D. Bi, W. Tress, M.I. Dar, P. Gao, J. Luo, C. Renevier, K. Schenk, A. Abate, F. Giordano, J.P. Correa Baena, J.D. Decoppet, S.M. Zakeeruddin, M.K. Nazeeruddin, M. Gratzel, A. Hagfeldt, Efficient luminescent solar cells based on tailored mixed-cation perovskites, Sci. Adv. 2 (2016) e1501170.
[6] M. Liu, M.B. Johnston, H.J. Snaith, Efficient planar heterojunction perovskite solar cells by vapour deposition, Nature 501 (2013) 395–398.
[7] W. Nie, H. Tsai, R. Asadpour, J.C. Blancon, A.J. Neukirch, G. Gupta, J.J. Crochet, M. Chhowalla, S. Tretiak, M.A. Alam, H.L. Wang, A.D. Mohite, High-efficiency solution-processed perovskite solar cells with millimeter-scale grains, Science 347 (2015) 522–525.
[8] N.J. Jeon, J.H. Noh, Y.C. Kim, W.S. Yang, S. Ryu, S. Seok II, Solvent engineering for high-performance inorganic-organic hybrid perovskite solar cells, Nat. Mater. 13 (2014) 897–903.
[9] J. Im, H. Kim, N. Park, Morphology-photovoltaic property correlation in perovskite solar cells: one-step versus two-step deposition of $CH_3NH_3PbI_3$, APL Mater. 2 (2014) 81510.
[10] N. Yantara, D. Sabba, F. Yanan, J.M. Kadro, T. Moehl, P.P. Boix, S. Mhaisalkar, M. Gratzel, C. Gratzel, Loading of mesoporous titania films by $CH_3NH_3PbI_3$ perovskite, single step vs. sequential deposition, Chem. Commun. 51 (2015) 4603–4606.
[11] H. Zhang, J. Mao, H. He, D. Zhang, H.L. Zhu, F. Xie, K.S. Wong, M. Gratzel, W.C.H. Choy, A smooth $CH_3NH_3PbI_3$ film via a new approach for forming the PbI_2 nanostructure together with strategically high CH_3NH_3I concentration for high efficient planar-heterojunction solar cells, Adv. Energy Mater. 5 (2015) 1501354.
[12] M.I. El-Henawey, R.S. Gebhardt, M.M. El-Tonsy, S. Chaudhary, Organic solvent vapor treatment of lead iodide layers in the two-step sequential deposition of $CH_3NH_3PbI_3$-based perovskite solar cells, J. Mater. Chem. A 4 (2016) 1947–1952.
[13] T. Zhang, M. Yang, Y. Zhao, K. Zhu, Controllable sequential deposition of planar $CH_3NH_3PbI_3$ perovskite films via adjustable volume expansion, Nano Lett. 15 (2015) 3959–3963.
[14] B.E. Cohen, S. Gamliel, L. Etgara, Parameters influencing the deposition of methylammonium lead halide iodide in hole conductor free perovskite-based solar cells, APL Mater. 2 (2014) 81502.
[15] H. Zheng, W. Wang, S. Yang, Y. Liu, J. Sun, A facile way to prepare nanoporous PbI_2 films and their application in fast conversion to $CH_3NH_3PbI_3$, RSC Adv. 6 (2016) 1611–1617.
[16] D.H. Cao, C.C. Stoumpos, C.D. Malliakas, M.J. Katz, O.K. Farha, J.T. Hupp, M.G. Kanatzidis, Remnant PbI_2, an unforeseen necessity in high-efficiency hybrid perovskite-based solar cells? APL Mater. 2 (2014) 91101.
[17] Z. Xiao, C. Bi, Y. Shao, Q. Dong, Q. Wang, Y. Yuan, C. Wang, Y. Gao, J. Huang, Efficient, high yield perovskite photovoltaic devices grown by interdiffusion of solution-processed precursor stacking layers, Energy Environ. Sci. 7 (2014) 2619–2623.
[18] Y. Zhou, M. Yang, A.L. Vasiliev, H.F. Garces, Y. Zhao, D. Wang, S. Pang, K. Zhu, N.P. Padture, Growth control of compact $CH_3NH_3PbI_3$ thin films via enhanced solid-state precursor reaction for efficient planar perovskite solar cells, J. Mater. Chem. A 3 (2015) 9249–9256.

[19] Z. Yang, B. Cai, B. Zhou, T. Yao, W. Yu, S.F. Liu, W. Zhang, C. Li, An up-scalable approach to $CH_3NH_3PbI_3$ compact films for high-performance perovskite solar cells, Nano Energy 15 (2015) 670–678.
[20] L. Chen, F. Tang, Y. Wang, S. Gao, W. Cao, J. Cai, L. Chen, Facile preparation of organometallic perovskite films and high-efficiency solar cells using solid-state chemistry, Nano Res. 8 (2015) 263–270.
[21] W. Peng, B. Anand, L. Liu, S. Sampat, B.E. Bearden, A.V. Malko, Y.J. Chabal, Influence of growth temperature on bulk and surface defects in hybrid lead halide perovskite films, Nanoscale 8 (2016) 1627–1634.
[22] Y. Wu, A. Islam, X. Yang, C. Qin, J. Liu, K. Zhang, W. Peng, L. Han, Retarding the crystallization of PbI_2 for highly reproducible planar-structured perovskite solar cells via sequential deposition, Energy Environ. Sci. 7 (2014) 2934–2938.
[23] J. Cao, F. Wang, H. Yu, Y. Zhou, H. Lu, N. Zhao, C. Wong, Porous PbI_2 films for the fabrication of efficient, stable perovskite solar cells via sequential deposition, J. Mater. Chem. A 4 (2016) 10223–10230.
[24] K. Liang, D.B. Mitzi, M.T. Prikas, Synthesis and characterization of organic-inorganic perovskite thin films prepared using a versatile two-step dipping technique, Chem. Mater. 10 (1998) 403–411.
[25] Q. Chen, H. Zhou, Z. Hong, S. Luo, H. Duan, H. Wang, Y. Liu, G. Li, Y. Yang, Planar heterojunction perovskite solar cells via vapor-assisted solution process, J. Am. Chem. Soc. 136 (2014) 622–625.
[26] H. Mehrer, Diffusion in Solids: Fundamentals, Methods, Materials, Diffusion-Controlled Processes, first ed., Springer-Verlag, Heidelberg, Berlin, 2007.
[27] T. Liu, Q. Hu, J. Wu, K. Chen, L. Zhao, F. Liu, C. Wang, H. Lu, S. Jia, T. Russell, R. Zhu, Q. Gong, Mesoporous PbI_2 scaffold for high-performance planar heterojunction perovskite solar cells, Adv. Energy Mater. 6 (2016) 1501890.
[28] H. Ko, J. Lee, N. Park, 15.76% efficiency perovskite solar cells prepared under high relative humidity: importance of PbI_2 morphology in two-step deposition of $CH_3NH_3PbI_3$, J. Mater. Chem. A 3 (2015) 8808–8815.
[29] Y. Zhou, M. Yang, J. Kwun, O.S. Game, Y. Zhao, S. Pang, N.P. Padture, K. Zhu, Intercalation crystallization of phase-pure Alpha-HC-$(NH_2)_2PbI_3$ upon microstructurally engineered PbI_2 thin films for planar perovskite solar cells, Nanoscale 8 (2016) 6265–6270.
[30] H. Xue, X. Kong, Z. Liu, C. Liu, J. Zhou, W. Chen, S. Ruan, Q. Xu, TiO_2 based metal-semiconductor-metal ultraviolet photodetectors, Appl. Phys. Lett. 90 (2007) 201118.
[31] Q. Chen, H. Zhou, T. Song, S. Luo, Z. Hong, H. Duan, L. Dou, Y. Liu, Y. Yang, Controllable self-induced passivation of hybrid lead iodide perovskites toward high performance solar cells, Nano Lett. 14 (2014) 4158–4163.
[32] T. Zhang, N. Guo, G. Li, X. Qian, Y. Zhao, A controllable fabrication of grain boundary PbI_2 nanoplates passivated lead halide perovskites for high performance solar cells, Nano Energy 26 (2016) 50–56.
[33] Y. Zhao, A.M. Nardes, K. Zhu, Mesoporous perovskite solar cells: material composition, charge-carrier dynamics, and device characteristics, Faraday Discuss. 176 (2014) 301–312.
[34] Y.H. Lee, J. Luo, R. Humphry-Baker, P. Gao, M. Grätzel, M.K. Nazeeruddin, Unraveling the reasons for efficiency loss in perovskite solar cells, Adv Funct. Mater. 25 (2015) 3925–3933.
[35] Z. Xiao, Q. Dong, C. Bi, Y. Shao, Y. Yuan, J. Huang, Solvent annealing of perovskite-induced crystal growth for photovoltaic-device efficiency enhancement, Adv. Mater. 26 (2014) 6503–6509.
[36] A.R. Pascoe, N.W. Duffy, A.D. Scully, F. Huang, Y. Cheng, Insights into planar $CH_3NH_3PbI_3$ perovskite solar cells using impedance spectroscopy, J. Phys. Chem. C 119 (2015) 4444–4453.
[37] F. Liu, Q. Dong, M.K. Wong, A.B. Djurišić, A. Ng, Z. Ren, Q. Shen, C. Surya, W.K. Chan, J. Wang, A.M.C. Ng, C. Liao, H. Li, K. Shih, C. Wei, H. Su, J. Dai, Is excess PbI_2 beneficial for perovskite solar cell performance? Adv. Energy Mater. 6 (2016) 1502206.
[38] Y. Han, S. Meyer, Y. Dkhissi, K. Weber, J.M. Pringle, U. Bach, L. Spiccia, Y. Cheng, Degradation observations of encapsulated planar $CH_3NH_3PbI_3$ perovskite solar cells at high temperatures and humidity, J. Mater. Chem. A 3 (2015) 8139–8147.
[39] Y. Jeon, S. Lee, R. Kang, J. Kim, J. Yeo, S. Lee, S. Kim, J. Yun, D. Kim, Planar heterojunction perovskite solar cells with superior reproducibility, Sci. Rep. 4 (2014) 6953.
[40] T. Baikie, Y. Fang, J.M. Kadro, M. Schreyer, F. Wei, S.G. Mhaisalkar, M. Gratzel, T.J. White, Synthesis and crystal chemistry of the hybrid perovskite $(CH_3NH_3)PbI_3$ for solid-state sensitised solar cell applications, J. Mater. Chem. A 1 (2013) 5628–5641.
[41] C. Bi, Y. Shao, Y. Yuan, Z. Xiao, C. Wang, Y. Gao, J. Huang, Understanding the formation and evolution of interdiffusion grown organolead halide perovskite thin films by thermal annealing, J. Mater. Chem. A 2 (2014) 18508–18514.
[42] J. Shi, Y. Luo, H. Wei, J. Luo, J. Dong, S. Lv, J. Xiao, Y. Xu, L. Zhu, X. Xu, H. Wu, D. Li, Q. Meng, Modified two-step deposition method for high-efficiency $TiO_2/CH_3NH_3PbI_3$ heterojunction solar cells, ACS Appl. Mater. Interfaces 6 (2014) 9711–9718.
[43] T. Salim, S. Sun, Y. Abe, A. Krishna, A.C. Grimsdale, Y.M. Lam, Perovskite-based solar cells: impact of morphology and device architecture on device performance, J. Mater. Chem. A 3 (2015) 8943–8969.
[44] H.J. Snaith, A. Abate, J.M. Ball, G.E. Eperon, T. Leijtens, N.K. Noel, S.D. Stranks, J.T. Wang, K. Wojciechowski, W. Zhang, Anomalous hysteresis in perovskite solar cells, J. Phys. Chem. Lett. 5 (2014) 1511–1515.
[45] H. Chen, N. Sakai, M. Ikegami, T. Miyasaka, Emergence of hysteresis and transient ferroelectric response in organo-lead halide perovskite solar cells, J. Phys. Chem. Lett. 6 (2015) 164–169.